ACS chemical biology

pubs.acs.org/acschemicalbiology

Articles

Fluorescence Lifetime Imaging of pH along the Secretory Pathway

Peter T. A. Linders, Melina Ioannidis, Martin ter Beest, and Geert van den Bogaart*

Cite This: *ACS Chem. Biol.* 2022, 17, 240−251

Read Online

ACCESS | Metrics & More | Article Recommendations | Supporting Information

ABSTRACT: Many cellular processes are dependent on correct pH levels, and this is especially important for the secretory pathway. Defects in pH homeostasis in distinct organelles cause a wide range of diseases, including disorders of glycosylation and lysosomal storage diseases. Ratiometric imaging of the pH-sensitive mutant of green fluorescent protein, pHLuorin, has allowed for targeted pH measurements in various organelles, but the required sequential image acquisition is intrinsically slow and therefore the temporal resolution is unsuitable to follow the rapid transit of cargo between organelles. Therefore, we applied fluorescence lifetime imaging microscopy (FLIM) to measure intraorganellar pH with just a single excitation wavelength. We first validated this method by confirming the pH in multiple compartments along the secretory pathway and compared the pH values obtained by the FLIM-based measurements with those obtained by conventional ratiometric imaging. Then, we analyzed the dynamic pH changes within cells treated with Bafilomycin A1, to block the vesicular ATPase, and Brefeldin A, to block endoplasmic reticulum (ER)−Golgi trafficking. Finally, we followed the pH changes of newly synthesized molecules of the inflammatory cytokine tumor necrosis factor-α while they were in transit from the ER via the Golgi to the plasma membrane. The toolbox we present here can be applied to measure intracellular pH with high spatial and temporal resolution and can be used to assess organellar pH in disease models.

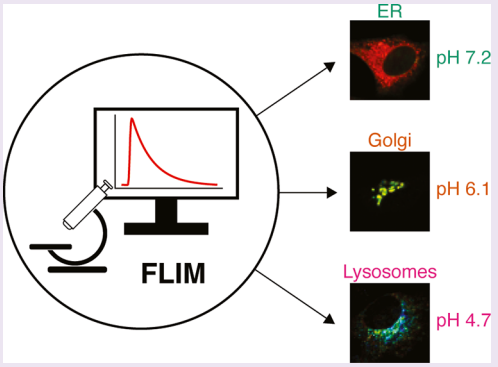

INTRODUCTION

Physiological pH homeostasis is crucial for many cellular processes. Not only the cytosolic pH is of importance, but defined intraorganellar pH delineates the secretory pathway. The pH of the endoplasmic reticulum (ER) is approximately 7, while the Golgi apparatus slightly acidifies from pH 6.7 at the cis face to pH 6.0 at the trans face.[1−3] Before secretory cargo is released at the plasma membrane and reaches the neutral pH of the extracellular environment, the pH in secretory vesicles is about 5.2.[1,2]

pH is not only crucial for proper protein folding and enzyme activity through influencing the charge of amino acid side chains, but its importance in secretory protein transport is increasingly clear.[4] pH affects binding affinities of cargo molecules to trafficking chaperones and thereby pH differences facilitate intracellular transport by both influencing the transit of cargo[5−11] and the sorting of secretory pathway resident proteins.[12−14] Moreover, the localization of glycosylation enzymes and their substrates is determined by pH,[4,15−18] and defects in this homeostasis cause a wide range of human disease.[4,19−25] Being able to accurately determine intraorganellar pH along the secretory pathway is, therefore, of both fundamental and diagnostic importance.

Fluorescent dyes that allow the measurement of intraorganellar pH exist and are commercially available,[26−30] but the inability of specific organellar targeting is a major drawback. The pH in the lumen of the Golgi and ER in mammalian cells has been measured using Shiga-like toxins covalently bound to fluorescent dyes[31,32] and with the biotin−avidin system.[33] However, especially the development of pH-sensitive mutants of green fluorescent protein (GFP), such as pHLuorin,[34,35] which can be targeted to specific organelles by fusion proteins, has enabled specific measurement of intracellular compartments. Two classes of pHLuorin were developed by mutagenesis, which altered the bimodal excitation spectrum of GFP with peaks at 395 and 475 nm.[34,36] First, ecliptic pHLuorin, which shows a reduction of its excitation efficiency at 475 nm at pH values lower than 6. Second, ratiometric pHLuorin, which shows a gradual increase in the ratio of excitation at 475/395 nm between pH 5.5 and pH 7.5.[34] With ecliptic pHLuorin, intraorganellar pH can be determined by first recording an image at 475 nm excitation and then correlating the fluorescence intensities with a calibration curve. The pH can be determined with ratiometric pHLuorin using a similar approach, but now by sequentially recording images at 395 and 475 nm excitation. A new version of ratiometric pHLuorin, ratiometric pHLuorin2

Received: November 18, 2021
Accepted: December 28, 2021
Published: January 10, 2022

https://doi.org/10.1021/acschembio.1c00907
ACS Chem. Biol. 2022, 17, 240−251

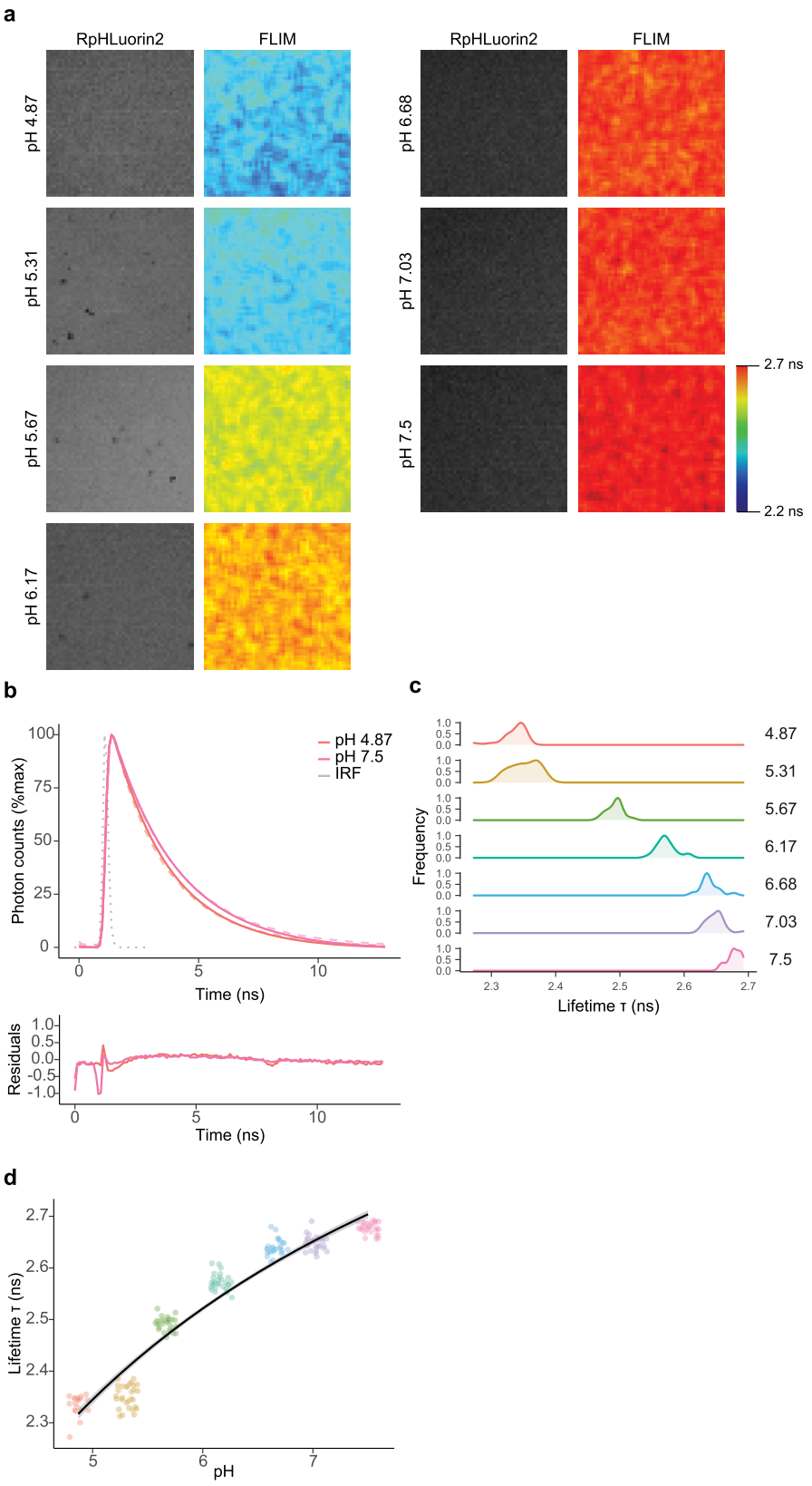

Figure 1. FLIM of recombinant RpHLuorin2. (a) Representative confocal images of 10 μM recombinant RpHLuorin2 in calibration buffers with defined pH. The intensity image (left column) was convoluted with the fluorescence lifetime value per pixel and pseudo-colored (right column). (b) Representative fluorescence lifetime histograms of recombinant RpHLuorin2 in pH 4.87 solution (red-dashed line) or pH 7.5 solution (pink-dashed line). Fits with monoexponential decay functions (pH 4.87, solid red line; pH 7.5, solid pink line) convoluted with the instrumental response function (gray-dotted line). Graphs are normalized to the maximum photon counts. (c) Average lifetime histograms from the images of panel (a). 30 regions of interest (i.e., ~10 × 10 μm of imaged area) were selected per pH buffer and the average lifetime τ was measured. (d) pH dependence of recombinant RpHLuorin2 in defined pH calibration buffers from the images of panel (a).

https://doi.org/10.1021/acschembio.1c00907
ACS Chem. Biol. 2022, 17, 240−251

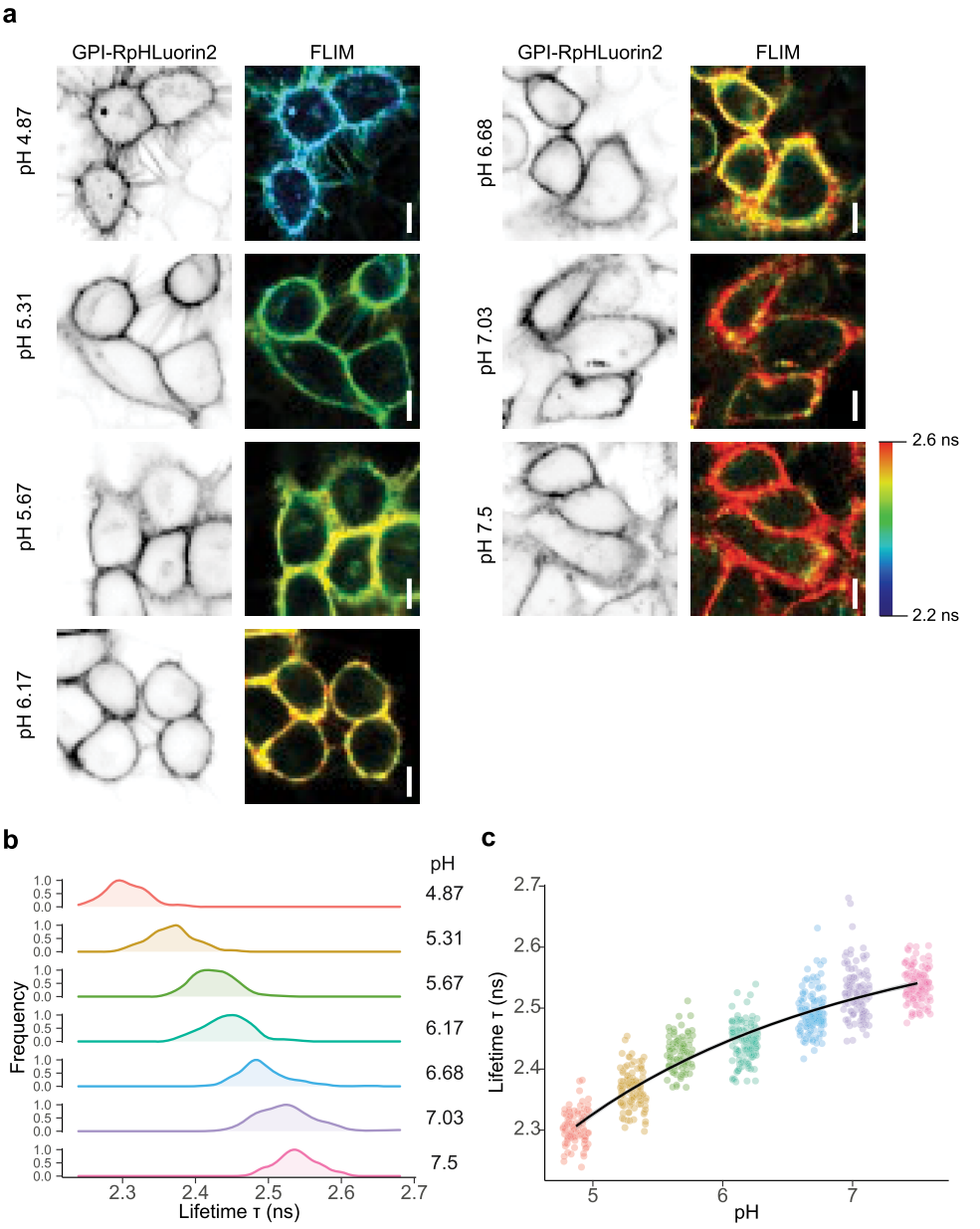

Figure 2. Calibration of RpHLuorin2 by FLIM in HeLa cells expressing GPI-RpHLuorin2. (a) Representative confocal micrographs of HeLa cells expressing GPI-RpHLuorin2 in defined calibration buffers. The intensity image (left column) was convoluted with the fluorescent lifetime value per pixel and pseudo-colored (right column). Scale bars, 10 μm. (b) Average lifetime histograms from the images of panel (a). $N = 86$ (pH 4.87), 108 (pH 5.31), 90 (pH 5.67), 115 (pH 6.17), 122 (pH 6.68), 113 (pH 7.03), and 120 (pH 7.5) cells from three independent experiments. (c) pH dependence of HeLa cells expressing GPI-RpHLuorin2 in defined pH calibration buffers from the images of panel (a).

(RpHLuorin2), was later developed with 8-fold improved fluorescence.[35]

Ecliptic pHLuorin is less accurate than ratiometric pHLuorin because the fluorescence intensity not only depends on the pH but also on the concentration of pHLuorin. However, ratiometric imaging also has several drawbacks, such as sensitivity to background fluorescence leading to high variations in the ratio values and the need for two sequential image acquisitions with two different excitation wavelengths. As the exocytic pathway is highly dynamic, the sequential imaging could potentially result in misalignment of the emitted signal (e.g., due to movement of organelles), compromising the calculation of ratio values. To overcome this problem of dual excitation, GFP-based probes have been developed that show a pH-dependent change in fluorescence emission, including E^2GFP[37] and deGFP4,[38,39] and pH-sensitive fluorophores have been targeted to organelles with the HaloTag technology.[40] However, spectral overlap in fluorescence emission wavelengths limits the use of these probes for multicolor experiments together with other fluorescent probes.

In this study, we used another approach to overcome the problem of dual excitation and exploit fluorescence lifetime, an intrinsic property of fluorophores that is insensitive to changes in laser intensity or protein concentration[41,42] but is sensitive to pH,[43,44] to accurately measure intraorganellar pH with both high spatial and temporal resolution.

RESULTS AND DISCUSSION

FLIM of Recombinant Ratiometric pHLuorin2. We first measured the fluorescence excitation spectra of recombinant

https://doi.org/10.1021/acschembio.1c00907
ACS Chem. Biol. 2022, 17, 240−251

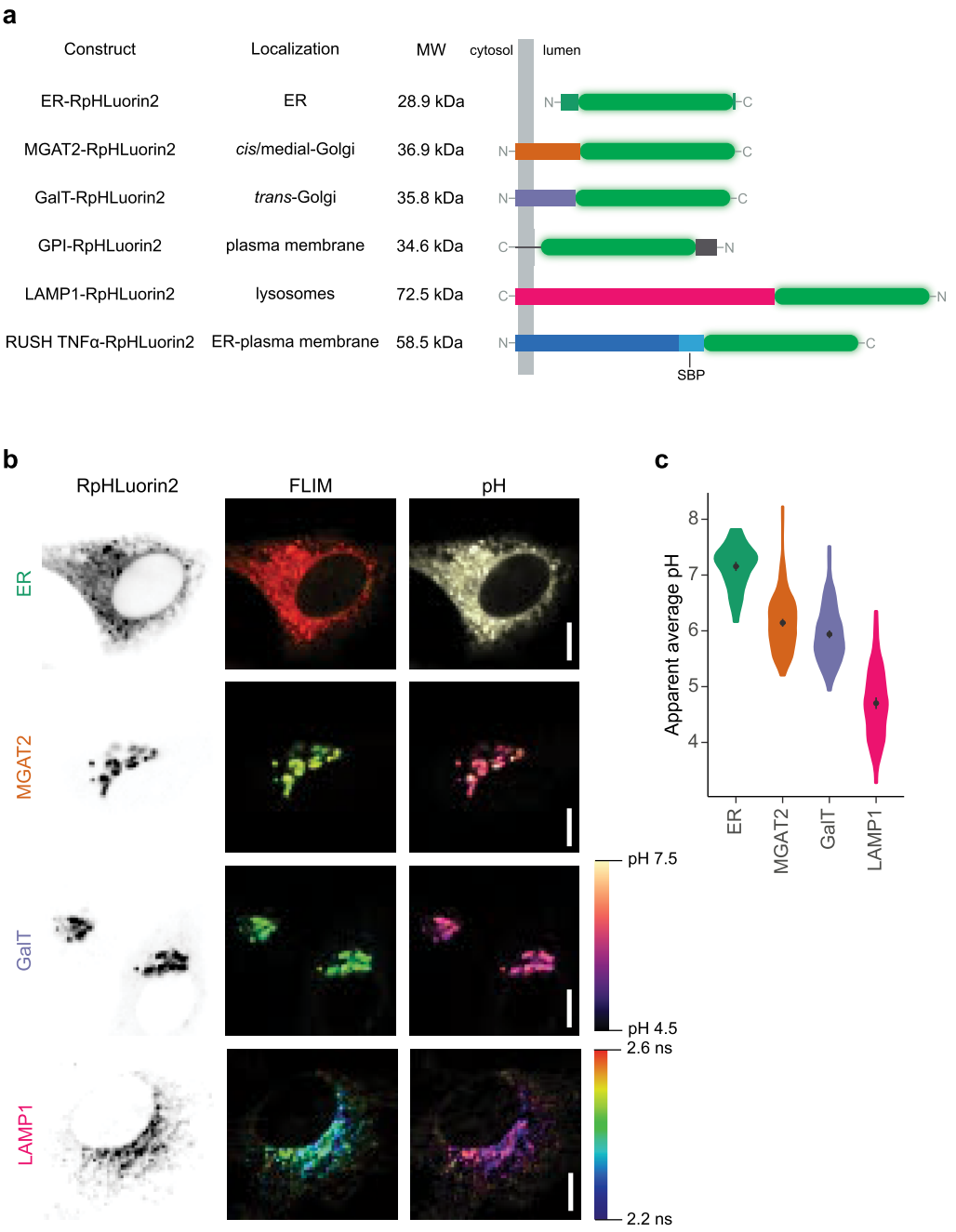

Figure 3. Steady-state pH measurements of secretory pathway markers. (a) Schematic overview of all RpHLuorin2 constructs used in this study. The signal sequence of LAMP1 is removed following cotranslational ER insertion and is not shown in the diagram. ER-RpHLuorin2 contains the N-terminal signal sequence of the ER-resident protein calreticulin and a C-terminal ER retention signal KDEL. MW: molecular weight; RUSH: retention using selective hooks;[51] and SBP: streptavidin-binding protein. (b) Representative confocal micrographs of HeLa cells expressing the mentioned RpHLuorin2 fusion constructs. The intensity image (left column) was convoluted with the fluorescent lifetime value per pixel and pseudo-colored (middle column). The intensity image was also convoluted with the calculated pH per pixel and pseudo-colored (right column). FLIM: fluorescence lifetime imaging microscopy. Scale bars, 10 μm. (c) Quantification of average pH values from panel (b). $N = 88$ (ER), 188 (MGAT2), 193 (GalT), and 134 (LAMP1) cells from three to five independent experiments.

RpHLuorin2 (Supporting Information Figure S1) in different pH solutions with a fluorescence spectrometer. Depending on the pH of the medium, the *p*-hydroxybenzylidene-imidazolidinone moiety in the chromophore of pHLuorin2, a derivative of GFP,[35] can exist in either the neutral phenol form or the anionic phenolate form.[45] As expected,[34] we observed strong dependence of the excitation efficiencies on pH, as a higher pH resulted in an increased emission brightness (at 508 nm) at an excitation wavelength of 470 nm, whereas the fluorescence brightness was reduced at an excitation wavelength of 405 nm (Supporting Information Figure S1a). These data show that for pHLuorin2, the anionic form shows an excitation peak at 405 nm, while the peak with 470 nm corresponds to the neutral form. We then plotted the ratios of the emission signals with 405 nm over 470 nm excitation as a function of the pH and fitted these data with a dose−response relationship, an empirical model to fit the sigmoidal data as the (de)protonation states of RpHLuorin2 will saturate at very high and low pH values (Supporting Information

https://doi.org/10.1021/acschembio.1c00907
ACS Chem. Biol. 2022, 17, 240−251

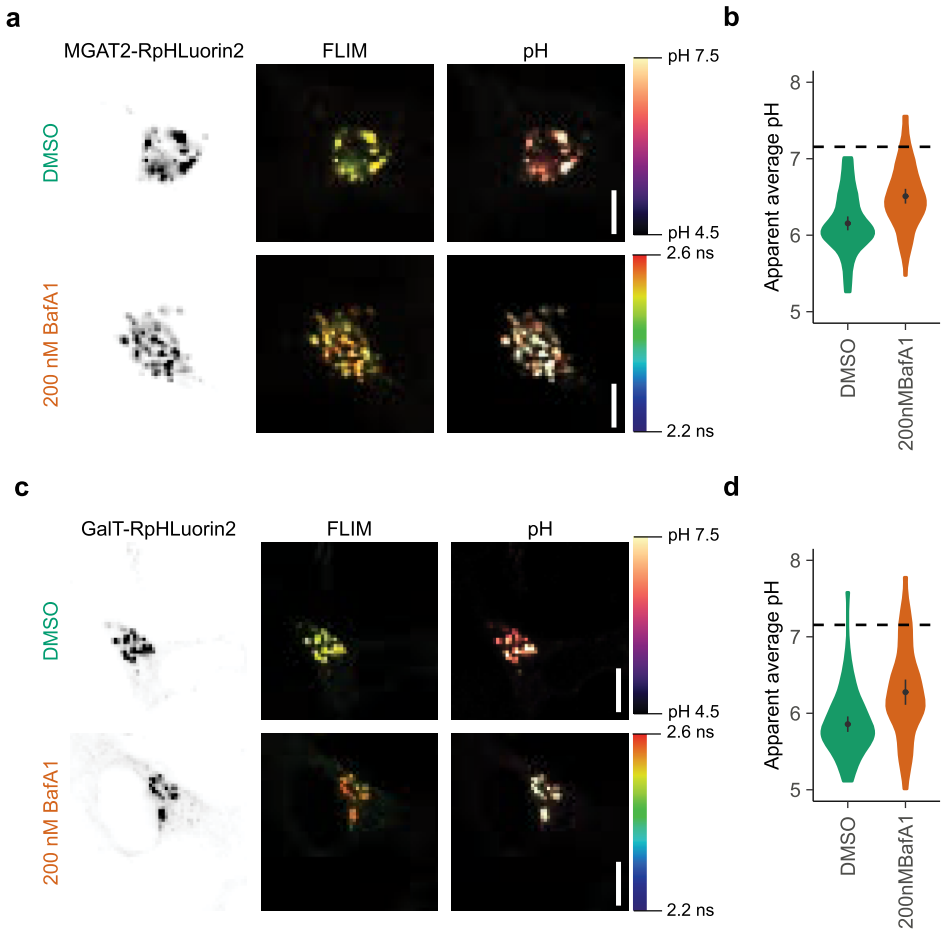

Figure 4. Incomplete blockage of Golgi acidification by Bafilomycin A1. (a) Representative confocal micrographs of HeLa cells expressing MGAT2-RpHLuorin2 incubated for 1 h in the absence (solvent control DMSO) or presence of Bafilomycin A1 (200 nM BafA1). To generate the FLIM images (middle column), the intensity images (left column) were convoluted with the fluorescent lifetime value per pixel and pseudo-colored. To generate the pH images, the lifetimes were converted to the calculated pH per pixel and also convoluted with the fluorescence intensities (right column). Scale bars, 10 μm. (b) Quantification of average pH values from panel (a). $N = 72$ (DMSO) and 77 (BafA1) cells from four independent experiments. The dashed lines indicate the average pH of the ER from Figure 3c. (c,d) Same as panels (a,b), but now for GalT-RpHLuorin2. $N = 68$ (DMSO) and 50 (BafA1A) cells from four independent experiments.

Figure S1b). The largest changes in fluorescence of RpHLuorin2 were observed between pH 5.5 and pH 7, making RpHLuorin2 an excellent candidate for pH measurements in the secretory pathway.

As ratiometric determination of pH with RpHLuorin2 requires two sequential image acquisitions with different excitation wavelengths, we investigated whether time-correlated single-photon counting fluorescence lifetime imaging microscopy (FLIM) would be an appropriate substitute to allow for single-scan imaging. We hypothesized that as the lifetime of fluorophores is influenced by pH,[43,44] the pH sensitivity of RpHLuorin2 would allow for accurate pH measurement based on fluorescence lifetime. Therefore, we performed FLIM of recombinant RpHLuorin2 in different pH solutions at 488 nm excitation (Figure 1). For GFP, the fluorescence lifetime of the phenolate form is in the 2−3 ns range, while that of the phenol form is <100 ps.[46,47] At 488 nm excitation, we will mainly excite the (fast) phenol form, but (due to fluorescence cross-talk) there will also be some contribution of the (slow) phenolate form. The observed fluorescence lifetime can hence be regarded as a mixture of the decays of the neutral and anionic forms. Thus, an increase in pH will result in a net higher lifetime, as has been reported for other GFP-derived fluorescent proteins.[43,48]

For purified recombinant pHLuorin2, we observed a dependency of the lifetime as a function of pH, and the fluorescence lifetime increased upon an increasing pH (Figure 1). However, the fluorescence lifetime changed over a larger range of pH values (4.5−7.5; Figure 1d) than the ratio of 405/470 nm excitations (5.5−7.5; Supporting Information Figure S1b). This larger dynamic range, which is likely caused by a second protonation event, is an advantage of the FLIM-based approach, because it increases the range of pH values that can be determined. We then fused RpHLuorin2 to several intraorganellar markers in the secretory pathway to perform pH measurements in living cells.

pH Measurements in the Secretory Pathway. In order to accurately measure intraorganellar pH of specific organelles, we targeted RpHLuorin2 intracellularly by fusing it to proteins and targeting sequences that locate to specific subcellular locations in the secretory pathway (Figure 3a). The pH range that can be measured with lifetime-based measurements of pHLuorin2 (4.5−7.5) is ideally suited for measuring pH along the secretory pathway, as the pH is neutral within the ER (~7), slightly acidic (~6) in the Golgi network, and about 5.2 in secretory vesicles.[1−3] To interrogate the luminal pH along the entire secretory pathway, we fused RpHLuorin2 to the signal

https://doi.org/10.1021/acschembio.1c00907
ACS Chem. Biol. 2022, 17, 240−251

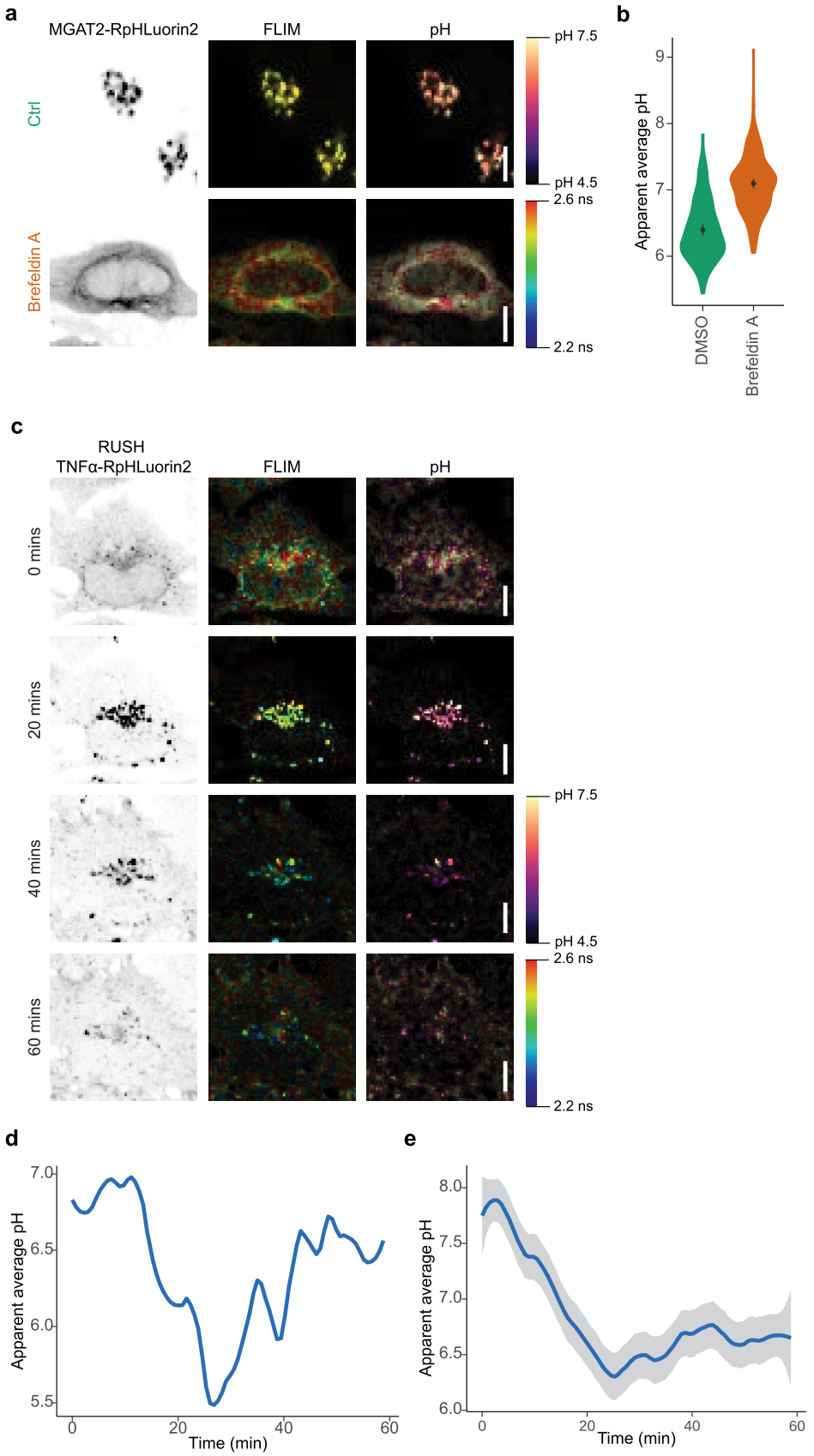

Figure 5. Dynamic pH measurements along the secretory pathway. (a) Representative confocal micrographs of HeLa cells expressing MGAT2-RpHLuorin2 in the absence (Ctrl, green) or presence of BFA (orange). The intensity image (left column) was convoluted with the fluorescent lifetime value per pixel and pseudo-colored (middle column). The intensity image was also convoluted with the calculated pH per pixel and pseudo-colored (right column). FLIM, fluorescence lifetime imaging microscopy. Scale bars, 10 μm. (b) Quantification of average pH values from panel (a). $N = 110$ (DMSO) and 165 (BFA) cells from 2−3 independent experiments. (c) Representative confocal micrographs of HeLa cells expressing RUSH TNFα-

https://doi.org/10.1021/acschembio.1c00907
ACS Chem. Biol. 2022, 17, 240−251

Figure 5. continued

RpHLuorin2 in the absence of biotin (0 min) or 20, 40, and 60 min after biotin addition. The intensity image (left column) was convoluted with the fluorescent lifetime value per pixel and pseudo-colored (middle column). The intensity image was also convoluted with the calculated pH per pixel and pseudo-colored (right column). FLIM, fluorescence lifetime imaging microscopy. Scale bars, 10 μm. See also Supporting Information Movie S1. (d) Quantification of average pH values of the cell shown in panel (c) and Supporting Information Movie S1. Plotted is the average apparent lifetime for all pixels of the projected imaged area of the cell. (e) Average pH measured of all cells expressing RUSH TNFα-RpHLuorin2. N = 29 from two independent experiments.

sequence of the ER-resident protein calreticulin and a C-terminal ER retention signal KDEL for ER targeting, to the luminal regions of cis-/medial-Golgi protein alpha-1,6-mannosyl-glycoprotein 2-beta-*N*-acetylglucosaminyltransferase (MGAT2), to trans-Golgi enzyme beta-1,4-galactosyltransferase 1 (GalT), to trans-Golgi network protein TGN46, and to lysosome-associated membrane glycoprotein 1 (LAMP1) for lysosomal targeting, and finally to a GPI anchor for plasma membrane (i.e., extracellular) localization. For the Golgi enzymes (MGAT2 and GalT), we truncated each protein by removing their catalytic sites and only kept the transmembrane region and stalk regions responsible for their localization.[49−51]

We then expressed the fusion constructs in HeLa cells, and recorded FLIM images. We used the GPI-anchored RpHLuorin2 (GPI-RpHLuorin2) to calibrate the probe expressed in cells using the same pH buffers as used for the calibration of purified RpHLuorin2 (Figure 2). We again observed a dependency of the fluorescence lifetime of RpHLuorin2 on pH, although the absolute fluorescence lifetime values were lower than for the recombinant RpHLuorin2, possibly due to crowding effects leading to fluorescence self-quenching[52] and/or to differences in the local microenvironment such as phospholipid charge and microdomain pH. These effects, as well as intracellular pools of GPI-pHLuorin2, likely also contributed to the variation among cells. The fluorescence lifetime dependency on pH could again be fitted with a sigmoidal dose−response model.

After successfully calibrating our system, we proceeded with pH measurements in the lumen of the organelles along of the secretory pathway (Figure 3). With ER-RpHLuorin2, we measured an apparent average pH of 7.2 [95% confidence interval (CI) ± 0.08], while with medial-Golgi marker MGAT2-RpHLuorin2, we measured an apparent average pH of 6.1 (95% CI ± 0.07), and with trans-Golgi marker GalT-RpHLuorin2, an apparent average pH of 5.9 (95% CI ± 0.07) (Figure 3b,c). Finally, for lysosomal marker LAMP1-RpHLuorin2, we measured an apparent average pH of 4.7 (95% CI ± 0.15) (Figure 3b,c). These pH values are all consistent with previous literature.[1,26] The fluorescence intensities (numbers of photons collected per cell) did not correlate with the fluorescence lifetimes for the four measured probes (Supporting Information Figure S2), indicating that intercellular variations were not caused by differences in expression levels.

To compare the FLIM-based measurements with ratiometric measurements, we also performed ratiometric imaging in cells using confocal laser scanning microscopy, where we changed the excitation wavelength of each line of the imaging (Supporting Information Figure S3). Confirming our previous experiments with purified RpHLuorin2 (Figure 1; Supporting Information Figure S1), we observed for GPI-pHLuorin2 that the ratio of fluorescence with 405 and 488 nm excitations changed over a narrower range of pH values (5.5−7.5; Supporting Information Figure S3a) than with FLIM imaging (4.5−7.5; Figure 2). For the MGAT2 and GalT probes, we observed similar pH values to the FLIM-based measurements [Supporting Information Figure S3b; MGAT2 pH 6.5 (95% CI ± 0.16), GalT pH 6.1 (95% CI ± 0.13)]. However, the spread of the data was considerably (∼2-fold) larger for the ratiometric approach. As a result, less cells have to be analyzed with the FLIM-based approach to accurately determine the pH. To illustrate this point, we performed Bootstrap statistical analysis, where we sampled our datasets to estimate the 95% CI based on samples of increasing numbers of cells (Supporting Information Figure S4). Based on this analysis, we estimate that for the FLIM-based approach, >16 cells needed to be measured for an accurate estimation of the pH for the ER, MGAT2, GalT, and LAMP1 markers. However, for the ratiometric approach, approximately 2-fold more cells needed to be analyzed to reach a similar 95% CI.

To further characterize the RpHLuorin2 FLIM system, we challenged cells with the vacuolar H^+-ATPase (V-ATPase) inhibitor Bafilomycin A1 (BafA1).[53] The mammalian V-ATPase is a protein pump that acidifies intraorganellar lumina by translocating protons across the membrane.[54,55] Our experiments with the MGAT2 and GalT probes showed that challenging the cells for 1 h with 200 nM BafA1 resulted in a reduced acidification (i.e., less reduction of pH compared to without BafA1) of both the cis- and trans-Golgi apparatus, although this perturbation was incomplete as the pH did not reach completely neutral values (Figure 4). Taken together, our data show that the RpHLuorin2 FLIM system is highly suitable for intracellular pH measurements with only a single-image acquisition.

pH Dynamics along the Secretory Pathway. To evaluate whether our method would be able to measure dynamic changes in pH, we started by measuring the pH of the medial-Golgi marker MGAT2-pHLuorin2 in the presence of fungal metabolite Brefeldin A (BFA). BFA is a potent inhibitor of ER-Golgi trafficking and causes the relocation of Golgi-resident enzymes to the ER.[56,57] We, therefore, expected a substantial increase in pH when MGAT2-RpHLuorin2-expressing cells were challenged with BFA. Indeed, we measured an apparent average pH of 7.1 (95% CI ± 0.07) in the BFA-challenged cells compared to an apparent average pH of 6.4 (95% CI ± 0.08) in the vehicle control cells (Figure 5a,b). This result means that our system is capable of measuring dynamic alterations of pH in living cells.

Next, we employed FLIM-based measurements to monitor the changes of the pH in real-time along the secretory pathway. To this end, we chose the secreted cytokine tumor necrosis factor alpha (TNF-α) as a model protein that is transported through the secretory pathway. Using the retention using selective hooks (RUSH) system,[51] we synchronized the transit of TNF-α along the secretory pathway. RUSH uses the expression of two separate constructs in the cell: (i) the hook construct, which is an ER-targeting sequence fused to streptavidin and (ii) the reporter construct, which is the protein of interest (i.e., TNF-α) fused in tandem to a streptavidin-binding protein (SBP) and a fluorescent protein (RpHLuorin2). When biotin is absent from the culture medium, the reporter

https://doi.org/10.1021/acschembio.1c00907
ACS Chem. Biol. 2022, 17, 240−251

construct is held at the ER through an interaction of streptavidin of the hook construct and the SBP. When biotin is added to the culture medium, biotin outcompetes this interaction and the reporter construct is released and transits along the secretory pathway in a synchronized fashion.

In our case, we used the KDEL-motif as a targeting sequence for the ER,[51] and used a TNFα-SBP-RpHLuorin2 fusion protein (RUSH TNFα-SBP-RpHLuorin2) as the reporter construct, so that we could follow the dynamic transit of TNF-α from the ER, via the Golgi network, to the plasma membrane (Figure 5c−e, Supporting Information Movie S1). We confirmed the subcellular localizations with immunolabeling experiments, where we fixed cells expressing TNFα-SBP-RpHLuorin2 at discrete time intervals after biotin addition and immunolabeled for organellar markers for the ER (PDI), Golgi network (GM130), and plasma membrane (WGA) (Supporting Information Figure S5).

In the absence of biotin in the cell culture medium, when all the TNFα-SBP-RpHLuorin2 reporter construct was trapped within the ER, we measured an apparent average pH of 7.58 (95%CI ± 0.46) (Figure 5c−e, Supporting Information Movie S1). In the ∼25 min following the addition of biotin to the cells, TNFα-SBP-RpHLuorin2 was trafficked through the Golgi and the apparent average pH gradually decreased to around pH 6. At later time points, the pH gradually increased again as more TNFα-SBP-RpHLuorin2 reached the plasma membrane. As HeLa cells express the protease TACE, TNF-α likely dissociates from the plasma membrane.[58−60]

After biotin addition, the TNF-α-RpHLuorin2 became concentrated in the Golgi network, leading to a local increase of the signal at this position (Supporting Information Figure S6). In order to not saturate the signal at this timepoint, we had to use a low intensity of excitation light for the RUSH experiments. However, at the start of the experiments (i.e., prior to biotin addition), the TNF-α-RpHLuorin2 construct was located at the ER, which in mammalian cells is diffuse and scattered through the entire cytoplasm. Likely as a consequence, the photon count/pixel at earlier timepoints was low, leading to an overestimation of the pH particularly for the ER localization. Also because of the limited number of photons, we fitted the fluorescence lifetime histograms with a single exponential decay function and report the apparent average pH per cell.[61]

This result demonstrates that FLIM-based pH measurements are a suitable method to determine intraorganellar pH with high temporal resolution.

CONCLUSIONS

In this study, we measured the pH in various subcellular compartments using FLIM of the pH-sensitive fluorescent protein RpHLuorin2. Consistent with previous literature, we observed a clear acidification of luminal pH through the secretory pathway.[1−3] The fusion of RpHLuorin2 is not restricted to the proteins we described here; this system is applicable to any other intraorganellar measurement, provided that RpHLuorin2 can be fused to a luminal domain of a protein residing in the target organelle. Furthermore, additional applications include combining RpHLuorin2 with other fluorescence (lifetime)-based probes to measure pH and other cellular processes simultaneously within the same cell.

We also show that the FLIM approach enables measuring pH with a kinetic resolution high enough to follow the dynamic transit of a cargo molecule along the secretory pathway. In this respect, our approach complements measurements of the exocytic pathway using Vero and Shiga toxins labeled with pH-sensitive fluorophores.[31] These toxins are endocytosed by receptor-mediated endocytosis and then transit via the Golgi network to the ER, a process that can be followed by microscopy. While this approach also enables measuring pH along the secretory pathway, a disadvantage is that it does not allow following the pH of designated secretory targets. For example, after transit through the Golgi, TNF-α is reported to traffic via designated subcompartments of recycling endosomes to the plasma membrane,[62] and it is not known whether Shiga toxins also traffic via these compartments.

Compared to excitation-based ratiometric imaging, the key improvement of our study is the usage of FLIM. Ratiometric imaging of pHLuorin and derivatives[30,34,35] requires the sequential recording of the fluorescent protein at both 405 and 470 nm excitation wavelengths, while the emission is recorded at the same wavelength. Although certain optical schemes such as split-beam excitation might facilitate fast switching between excitation wavelengths, this sequential excitation intrinsically limits the temporal resolution and consequently limits the applicability for pH determination in dynamically moving and reshaping organelles. A problem with such ratiometric imaging is that if the molecules (or organelles) move or photobleach during the sequential excitation, this will lead to an error as it causes variation in the ratios of the fluorescence intensities of the two excitation channels. FLIM mitigates this issue, as only a single recording with a single excitation wavelength is required. Therefore, movement of fluorescent molecules and photobleaching are no problem, because the fluorescence lifetime is independent of the concentration of fluorophores. FLIM is hence better suited for visualizing the pH of organelles in living cells. Moreover, FLIM measurements are not dependent on laser intensity,[41,42] while ratiometric measurements can easily be affected by fluctuations in excitation laser power. FLIM measurements are thus more comparable between experiments, as supported by our findings that the spread in the data is larger for the ratiometric than for the FLIM approach. Another advantage of the FLIM-based approach is that reference measurements can be used over independent experiments because the fluorescence lifetime is independent of the fluorescence intensity.[41,42] This is an advantage over the ratiometric approach, where small differences in the laser intensity and alignment of the microscope can have a major effect. However, a disadvantage is that it requires access to a FLIM microscope, whereas ratiometric imaging can be performed on most of the confocal and epifluorescence microscopes.

In contrast to another study that relies on equilibrating pH with the ionophore monensin,[30] we used GPI-anchored RpHLuorin2 to obtain calibration curves with defined pH buffers because monensin is a known inhibitor of physiological Golgi transport, thereby likely affecting the observed fluorescence lifetime values.[63−69]

Defects in the regulation of pH are a hallmark of a wide range of disease, including disorders of glycosylation,[4,19,21−25] cancer,[70] neurodegenerative diseases,[71−74] mitochondrial disorders,[75] and lysosomal storage disorders.[76] The tools we presented in this study offer a method to assess intraorganellar pH using FLIM. Our data show that FLIM is more accurate than ratiometric imaging. Moreover, due to its high temporal resolution, it not only enables measuring pH in static compartments but also measuring the dynamic changes that a

https://doi.org/10.1021/acschembio.1c00907
ACS Chem. Biol. 2022, 17, 240−251

protein experiences during its trafficking along the secretory pathway.

METHODS

Microscopy. Time-correlated single-photon counting FLIM imaging was performed on a Leica SP8 SMD system at 37 °C, equipped with a HC PL APO CS2 63×/1.20 Water objective. pHLuorin2 was excited at 488 nm with a pulsed white light laser, operating at 80 MHz. Photons were collected for 1 min or 30 s for time-lapse experiments with a HyD detector set at 502−530 nm, and lifetime histograms of the donor fluorophore were fitted with a mono-exponential decay function convoluted with the microscope instrument response function in Leica LAS X. For reconstructing the images, tiff files with τ values were generated using FLIMFit[77] and 2 × 2 spatial binning and then convoluted with the fluorescence intensities using a custom-written ImageJ Macro. Ratiometric pH measurements were done similarly to the FLIM measurements, but the imaging was performed on a Leica SP8 SMD system at 37 °C, equipped with a HC PL APO CS2 63×/1.20 Water objective or a Zeiss LSM 800 system at 37 °C, equipped with a Plan Apochromat 1.4× Oil objective. RpHLuorin2 was excited at 405 and 488 nm sequentially, images were acquired with an emission wavelength bandwidth (495−560 nm) that included an emission wavelength of 508 nm.

See the Supporting Information for experimental details.

ASSOCIATED CONTENT

Supporting Information

The Supporting Information is available free of charge at https://pubs.acs.org/doi/10.1021/acschembio.1c00907.

Additional experimental details, materials, methods, and results, including control experiments for the ratiometric imaging, RUSH experiments, and statistical analysis; fluorescence excitation spectra of recombinant RpHLuorin2; FLIM-based pH measurements independent of expression intensity; measurements of organellar pH using ratiometric imaging of RpHLuorin 2; FLIM-based pH measurements more accurate than ratiometric pH measurements; colocalization of TNFa-SBP-RpHLuorin2 with organellar marker proteins; and fluorescence intensities during RUSH experiment (PDF)

Time-lapse FLIM imaging of RUSH TNFα-RpHLuorin2 in HeLa cells after biotin addition (AVI)

AUTHOR INFORMATION

Corresponding Author

Geert van den Bogaart − *Department of Tumor Immunology, Radboud Institute for Molecular Life Sciences, Radboud University Medical Center, 6525 GA Nijmegen, The Netherlands; Department of Molecular Immunology, Groningen Biomolecular Sciences and Biotechnology Institute, University of Groningen, 9747AG Groningen, Netherlands;* orcid.org/0000-0003-2180-6735; Phone: +31-50-36-35230; Email: g.van.den.bogaart@rug.nl

Authors

Peter T. A. Linders − *Department of Tumor Immunology, Radboud Institute for Molecular Life Sciences, Radboud University Medical Center, 6525 GA Nijmegen, The Netherlands;* orcid.org/0000-0003-2228-2822

Melina Ioannidis − *Department of Molecular Immunology, Groningen Biomolecular Sciences and Biotechnology Institute, University of Groningen, 9747AG Groningen, Netherlands*

Martin ter Beest − *Department of Tumor Immunology, Radboud Institute for Molecular Life Sciences, Radboud University Medical Center, 6525 GA Nijmegen, The Netherlands*

Complete contact information is available at: https://pubs.acs.org/10.1021/acschembio.1c00907

Author Contributions

P.T.A.L., M.t.B., and G.v.d.B. designed and performed the experiments and wrote the paper. M.I. performed the ratiometric pH measurements in HeLa cells and contributed to the writing of the paper.

Notes

The authors declare no competing financial interest.

All raw data, including R scripts and ImageJ macros, have been deposited to Zenodo.

ACKNOWLEDGMENTS

We thank the following people for constructs: H. Farhan and F. Perez (Str-KDEL_ManII-SBP-EGFP; Addgene plasmid #65252, Str-KDEL_TNF-SBP-EGFP; Addgene plasmid #65278), L. Lu (piRFP670-N1-GalT; Addgene plasmid #87325), C. Schultz and A. Nadler (GPI-mRFP), and E. Dell'Angelica (LAMP1-mGFP, Addgene plasmid #34831). We thank the Microscopy Imaging Center of the Radboud Institute for Molecular Life Sciences for use of their microscopy facilities. G.v.d.B. is funded by a Young Investigator Grant from the Human Frontier Science Program (HFSP; RGY0080/2018) and a Vidi grant from the Netherlands Organization for Scientific Research (NWO-ALW VIDI 864.14.001). G.v.d.B has also received funding from the European Research Council (ERC) under the European Union's Horizon 2020 research and innovation program (grant agreement no. 862137).

REFERENCES

(1) Casey, J. R.; Grinstein, S.; Orlowski, J. Sensors and Regulators of Intracellular PH. *Nat. Rev. Mol. Cell Biol.* **2010**, *11*, 50−61.

(2) Paroutis, P.; Touret, N.; Grinstein, S. The PH of the Secretory Pathway: Measurement, Determinants, and Regulation. *Physiology* **2004**, *19*, 207−215.

(3) Schapiro, F. B.; Grinstein, S. Determinants of the PH of the Golgi Complex. *J. Biol. Chem.* **2000**, *275*, 21025−21032.

(4) Linders, P. T. A.; Peters, E.; ter Beest, M.; Lefeber, D. J.; van den Bogaart, G. Sugary Logistics Gone Wrong: Membrane Trafficking and Congenital Disorders of Glycosylation. *Int. J. Mol. Sci.* **2020**, *21*, 4654.

(5) Appenzeller-Herzog, C.; Roche, A.-C.; Nufer, O.; Hauri, H.-P. PH-Induced Conversion of the Transport Lectin ERGIC-53 Triggers Glycoprotein Release. *J. Biol. Chem.* **2004**, *279*, 12943−12950.

(6) Vavassori, S.; Cortini, M.; Masui, S.; Sannino, S.; Anelli, T.; Caserta, I. R.; Fagioli, C.; Mossuto, M. F.; Fornili, A.; van Anken, E.; Degano, M.; Inaba, K.; Sitia, R. A PH-Regulated Quality Control Cycle for Surveillance of Secretory Protein Assembly. *Mol. Cell* **2013**, *50*, 783−792.

(7) Sannino, S.; Anelli, T.; Cortini, M.; Masui, S.; Degano, M.; Fagioli, C.; Inaba, K.; Sitia, R. Progressive Quality Control of Secretory Proteins in the Early Secretory Compartment by ERp44. *J. Cell Sci.* **2014**, *127*, 4260−4269.

(8) Watanabe, S.; Harayama, M.; Kanemura, S.; Sitia, R.; Inaba, K. Structural Basis of PH-Dependent Client Binding by ERp44, a Key Regulator of Protein Secretion at the ER−Golgi Interface. *Proc. Natl. Acad. Sci. U. S. A.* **2017**, *114*, E3224−E3232.

(9) Caplan, M. J.; Stow, J. L.; Newman, A. P.; Madri, J.; Anderson, H. C.; Farquhar, M. G.; Palade, G. E.; Jamieson, J. D. Dependence on PH of Polarized Sorting of Secreted Proteins. *Nature* **1987**, *329*, 632−635.

(10) Kokkonen, N.; Rivinoja, A.; Kauppila, A.; Suokas, M.; Kellokumpu, I.; Kellokumpu, S. Defective Acidification of Intracellular

Organelles Results in Aberrant Secretion of Cathepsin D in Cancer Cells. *J. Biol. Chem.* **2004**, *279*, 39982−39988.
(11) Kamiya, Y.; Kamiya, D.; Yamamoto, K.; Nyfeler, B.; Hauri, H.-P.; Kato, K. Molecular Basis of Sugar Recognition by the Human L-Type Lectins ERGIC-53, VIPL, and VIP36. *J. Biol. Chem.* **2008**, *283*, 1857−1861.
(12) Bräuer, P.; Parker, J. L.; Gerondopoulos, A.; Zimmermann, I.; Seeger, M. A.; Barr, F. A.; Newstead, S. Structural Basis for PH-Dependent Retrieval of ER Proteins from the Golgi by the KDEL Receptor. *Science* **2019**, *363*, 1103−1107.
(13) Wilson, D. W.; Lewis, M. J.; Pelham, H. R. PH-Dependent Binding of KDEL to Its Receptor in Vitro. *J. Biol. Chem.* **1993**, *268*, 7465−7468.
(14) Shibuya, A.; Margulis, N.; Christiano, R.; Walther, T. C.; Barlowe, C. The Erv41−Erv46 Complex Serves as a Retrograde Receptor to Retrieve Escaped ER Proteins. *J. Cell Biol.* **2015**, *208*, 197−209.
(15) Rivinoja, A.; Hassinen, A.; Kokkonen, N.; Kauppila, A.; Kellokumpu, S. Elevated Golgi PH Impairs Terminal N-Glycosylation by Inducing Mislocalization of Golgi Glycosyltransferases. *J. Cell. Physiol.* **2009**, *220*, 144−154.
(16) Hassinen, A.; Pujol, F. M.; Kokkonen, N.; Pieters, C.; Kihlström, M.; Korhonen, K.; Kellokumpu, S. Functional Organization of Golgi N- and O-Glycosylation Pathways Involves PH-Dependent Complex Formation That Is Impaired in Cancer Cells. *J. Biol. Chem.* **2011**, *286*, 38329−38340.
(17) Hassinen, A.; Kellokumpu, S. Organizational Interplay of Golgi N-Glycosyltransferases Involves Organelle Microenvironment-Dependent Transitions between Enzyme Homo- and Heteromers. *J. Biol. Chem.* **2014**, *289*, 26937−26948.
(18) Kellokumpu, S. Golgi PH, Ion and Redox Homeostasis: How Much Do They Really Matter? *Front. Cell Dev. Biol.* **2019**, *7*, 93.
(19) Kornak, U.; Reynders, E.; Dimopoulou, A.; van Reeuwijk, J.; Fischer, B.; Rajab, A.; Budde, B.; Nürnberg, P.; Foulquier, F.; Lefeber, D.; Urban, Z.; Gruenewald, S.; Annaert, W.; Brunner, H. G.; van Bokhoven, H.; Wevers, R.; Morava, E.; Matthijs, G.; Van Maldergem, L.; Mundlos, S. Impaired Glycosylation and Cutis Laxa Caused by Mutations in the Vesicular H + -ATPase Subunit ATP6V0A2. *Nat. Genet.* **2008**, *40*, 32−34.
(20) Morava, E.; Wopereis, S.; Coucke, P.; Gillessen-Kaesbach, G.; Voit, T.; Smeitink, J.; Wevers, R.; Grünewald, S. Defective Protein Glycosylation in Patients with Cutis Laxa Syndrome. *Eur. J. Hum. Genet.* **2005**, *13*, 414−421.
(21) Jansen, E. J. R.; Timal, S.; Ryan, M.; Ashikov, A.; van Scherpenzeel, M.; Graham, L. A.; Mandel, H.; Hoischen, A.; Iancu, T. C.; Raymond, K.; Steenbergen, G.; Gilissen, C.; Huijben, K.; van Bakel, N. H. M.; Maeda, Y.; Rodenburg, R. J.; Adamowicz, M.; Crushell, E.; Koenen, H.; Adams, D.; Vodopiutz, J.; Greber-Platzer, S.; Müller, T.; Dueckers, G.; Morava, E.; Sykut-Cegielska, J.; Martens, G. J. M.; Wevers, R. A.; Niehues, T.; Huynen, M. A.; Veltman, J. A.; Stevens, T. H.; Lefeber, D. J. ATP6AP1 Deficiency Causes an Immunodeficiency with Hepatopathy, Cognitive Impairment and Abnormal Protein Glycosylation. *Nat. Commun.* **2016**, *7*, 11600.
(22) Rujano, M. A.; Cannata Serio, M.; Panasyuk, G.; Péanne, R.; Reunert, J.; Rymen, D.; Hauser, V.; Park, J. H.; Freisinger, P.; Souche, E.; Guida, M. C.; Maier, E. M.; Wada, Y.; Jäger, S.; Krogan, N. J.; Kretz, O.; Nobre, S.; Garcia, P.; Quelhas, D.; Bird, T. D.; Raskind, W. H.; Schwake, M.; Duvet, S.; Foulquier, F.; Matthijs, G.; Marquardt, T.; Simons, M. Mutations in the X-Linked ATP6AP2 Cause a Glycosylation Disorder with Autophagic Defects. *J. Exp. Med.* **2017**, *214*, 3707−3729.
(23) Cannata Serio, M.; Graham, L. A.; Ashikov, A.; Larsen, L. E.; Raymond, K.; Timal, S.; Le Meur, G.; Ryan, M.; Czarnowska, E.; Jansen, J. C.; He, M.; Ficicioglu, C.; Pichurin, P.; Hasadsri, L.; Minassian, B.; Rugierri, A.; Kalimo, H.; Ríos-Ocampo, W. A.; Gilissen, C.; Rodenburg, R.; Jonker, J. W.; Holleboom, A. G.; Morava, E.; Veltman, J. A.; Socha, P.; Stevens, T. H.; Simons, M.; Lefeber, D. J. Mutations in the V-ATPase Assembly Factor VMA21 Cause a Congenital Disorder of Glycosylation With Autophagic Liver Disease. *Hepatology* **2020**, *72*, 1968−1986.
(24) Jansen, J. C.; Timal, S.; van Scherpenzeel, M.; Michelakakis, H.; Vicogne, D.; Ashikov, A.; Moraitou, M.; Hoischen, A.; Huijben, K.; Steenbergen, G.; van den Boogert, M. A. W.; Porta, F.; Calvo, P. L.; Mavrikou, M.; Cenacchi, G.; van den Bogaart, G.; Salomon, J.; Holleboom, A. G.; Rodenburg, R. J.; Drenth, J. P. H.; Huynen, M. A.; Wevers, R. A.; Morava, E.; Foulquier, F.; Veltman, J. A.; Lefeber, D. J. TMEM199 Deficiency Is a Disorder of Golgi Homeostasis Characterized by Elevated Aminotransferases, Alkaline Phosphatase, and Cholesterol and Abnormal Glycosylation. *Am. J. Hum. Genet.* **2016**, *98*, 322−330.
(25) Jansen, J. C.; Cirak, S.; van Scherpenzeel, M.; Timal, S.; Reunert, J.; Rust, S.; Pérez, B.; Vicogne, D.; Krawitz, P.; Wada, Y.; Ashikov, A.; Pérez-Cerdá, C.; Medrano, C.; Arnoldy, A.; Hoischen, A.; Huijben, K.; Steenbergen, G.; Quelhas, D.; Diogo, L.; Rymen, D.; Jaeken, J.; Guffon, N.; Cheillan, D.; van den Heuvel, L. P.; Maeda, Y.; Kaiser, O.; Schara, U.; Gerner, P.; van den Boogert, M. A. W.; Holleboom, A. G.; Nassogne, M.-C.; Sokal, E.; Salomon, J.; van den Bogaart, G.; Drenth, J. P. H.; Huynen, M. A.; Veltman, J. A.; Wevers, R. A.; Morava, E.; Matthijs, G.; Foulquier, F.; Marquardt, T.; Lefeber, D. J. CCDC115 Deficiency Causes a Disorder of Golgi Homeostasis with Abnormal Protein Glycosylation. *Am. J. Hum. Genet.* **2016**, *98*, 310−321.
(26) Johnson, D. E.; Ostrowski, P.; Jaumouillé, V.; Grinstein, S. The Position of Lysosomes within the Cell Determines Their Luminal PH. *J. Cell Biol.* **2016**, *212*, 677−692.
(27) D'Amore, C.; Orso, G.; Forgiarini, A.; Ceolotto, G.; Rennison, D.; Ribaudo, G.; Jay-Smith, M.; Hopkins, B.; Brimble, M. A.; Bova, S. Synthesis and Biological Characterization of a New Norbormide Derived Bodipy FL-Conjugated Fluorescent Probe for Cell Imaging. *Front. Pharmacol.* **2018**, *9*, 1055.
(28) Overly, C. C.; Lee, K. D.; Berthiaume, E.; Hollenbeck, P. J. Quantitative Measurement of Intraorganelle PH in the Endosomal-Lysosomal Pathway in Neurons by Using Ratiometric Imaging with Pyranine. *Proc. Natl. Acad. Sci. U. S. A.* **1995**, *92*, 3156−3160.
(29) Liu, H.; Song, W.; Gröninger, D.; Zhang, L.; Lu, Y.; Chan, K. S.; Zhou, Z.; Rurack, K.; Shen, Z. Real-Time Monitoring of Newly Acidified Organelles during Autophagy Enabled by Reaction-Based BODIPY Dyes. *Commun. Biol.* **2019**, *2*, 1−11.
(30) Ma, L.; Ouyang, Q.; Werthmann, G. C.; Thompson, H. M.; Morrow, E. M. Live-Cell Microscopy and Fluorescence-Based Measurement of Luminal PH in Intracellular Organelles. *Front. Cell Dev. Biol.* **2017**, *5*, 71.
(31) Kim, J. H.; Lingwood, C. A.; Williams, D. B.; Furuya, W.; Manolson, M. F.; Grinstein, S. Dynamic Measurement of the PH of the Golgi Complex in Living Cells Using Retrograde Transport of the Verotoxin Receptor. *J. Cell Biol.* **1996**, *134*, 1387−1399.
(32) Kim, J. H.; Johannes, L.; Goud, B.; Antony, C.; Lingwood, C. A.; Daneman, R.; Grinstein, S. Noninvasive Measurement of the PH of the Endoplasmic Reticulum at Rest and during Calcium Release. *Proc. Natl. Acad. Sci. U. S. A.* **1998**, *95*, 2997−3002.
(33) Wu, M. M.; Llopis, J.; Adams, S.; McCaffery, J. M.; Kulomaa, M. S.; Machen, T. E.; Moore, H.-P. H.; Tsien, R. Y. Organelle PH Studies Using Targeted Avidin and Fluorescein−Biotin. *Chem. Biol.* **2000**, *7*, 197−209.
(34) Miesenböck, G.; De Angelis, D. A.; Rothman, J. E. Visualizing Secretion and Synaptic Transmission with PH-Sensitive Green Fluorescent Proteins. *Nature* **1998**, *394*, 192−195.
(35) Mahon, M. J. PHluorin2: An Enhanced, Ratiometric, PH-Sensitive Green Florescent Protein. *Adv. Biosci. Biotechnol.* **2011**, *02*, 132−137.
(36) Ward, W. W.; Prentice, H. J.; Roth, A. F.; Cody, C. W.; Reeves, S. C. Spectral Perturbations of the Aequorea Green-Fluorescent Protein. *Photochem. Photobiol.* **1982**, *35*, 803−808.
(37) Bizzarri, R.; Arcangeli, C.; Arosio, D.; Ricci, F.; Faraci, P.; Cardarelli, F.; Beltram, F. Development of a Novel GFP-Based Ratiometric Excitation and Emission PH Indicator for Intracellular Studies. *Biophys. J.* **2006**, *90*, 3300−3314.

https://doi.org/10.1021/acschembio.1c00907
ACS Chem. Biol. 2022, 17, 240−251

(38) Hanson, G. T.; McAnaney, T. B.; Park, E. S.; Rendell, M. E. P.; Yarbrough, D. K.; Chu, S.; Xi, L.; Boxer, S. G.; Montrose, M. H.; Remington, S. J. Green Fluorescent Protein Variants as Ratiometric Dual Emission PH Sensors. 1. Structural Characterization and Preliminary Application. *Biochemistry* **2002**, *41*, 15477−15488.
(39) McAnaney, T. B.; Park, E. S.; Hanson, G. T.; Remington, S. J.; Boxer, S. G. Green Fluorescent Protein Variants as Ratiometric Dual Emission PH Sensors. 2. Excited-State Dynamics. *Biochemistry* **2002**, *41*, 15489−15494.
(40) Benink, H. A.; McDougall, M. G.; Klaubert, D. H.; Los, G. V. Direct PH Measurements by Using Subcellular Targeting of 5(and 6-) Carboxyseminaphthorhodafluor in Mammalian Cells. *BioTechniques* **2009**, *47*, 769−774.
(41) Wallrabe, H.; Periasamy, A. Imaging Protein Molecules Using FRET and FLIM Microscopy. *Curr. Opin. Biotechnol.* **2005**, *16*, 19−27.
(42) Jares-Erijman, E. A.; Jovin, T. M. FRET Imaging. *Nat. Biotechnol.* **2003**, *21*, 1387−1395.
(43) Schmitt, F.-J.; Thaa, B.; Junghans, C.; Vitali, M.; Veit, M.; Friedrich, T. EGFP-PHsens as a Highly Sensitive Fluorophore for Cellular PH Determination by Fluorescence Lifetime Imaging Microscopy (FLIM). *Biochim. Biophys. Acta, Bioenerg.* **2014**, *1837*, 1581−1593.
(44) Lin, H.-J.; Herman, P.; Lakowicz, J. R. Fluorescence Lifetime-Resolved PH Imaging of Living Cells. *Cytometry, Part A* **2003**, *52*, 77−89.
(45) Liu, Y.; Kim, H.-R.; Heikal, A. A. Structural Basis of Fluorescence Fluctuation Dynamics of Green Fluorescent Proteins in Acidic Environments. *J. Phys. Chem. B* **2006**, *110*, 24138−24146.
(46) Cotlet, M.; Hofkens, J.; Maus, M.; Gensch, T.; Van der Auweraer, M.; Michiels, J.; Dirix, G.; Van Guyse, M.; Vanderleyden, J.; Visser, A. J. W. G.; De Schryver, F. C. Excited-State Dynamics in the Enhanced Green Fluorescent Protein Mutant Probed by Picosecond Time-Resolved Single Photon Counting Spectroscopy. *J. Phys. Chem. B* **2001**, *105*, 4999−5006.
(47) Heikal, A. A.; Hess, S. T.; Webb, W. W. Multiphoton Molecular Spectroscopy and Excited-State Dynamics of Enhanced Green Fluorescent Protein (EGFP): Acid−Base Specificity. *Chem. Phys.* **2001**, *274*, 37−55.
(48) Nakabayashi, T.; Oshita, S.; Sumikawa, R.; Sun, F.; Kinjo, M.; Ohta, N. PH Dependence of the Fluorescence Lifetime of Enhanced Yellow Fluorescent Protein in Solution and Cells. *J. Photochem. Photobiol., A* **2012**, *235*, 65−71.
(49) Welch, L. G.; Munro, S. A Tale of Short Tails, through Thick and Thin: Investigating the Sorting Mechanisms of Golgi Enzymes. *FEBS Lett.* **2019**, *593*, 2452−2465.
(50) Tie, H. C.; Mahajan, D.; Chen, B.; Cheng, L.; VanDongen, A. M. J.; Lu, L. A Novel Imaging Method for Quantitative Golgi Localization Reveals Differential Intra-Golgi Trafficking of Secretory Cargoes. *Mol. Biol. Cell* **2016**, *27*, 848−861.
(51) Boncompain, G.; Divoux, S.; Gareil, N.; de Forges, H.; Lescure, A.; Latreche, L.; Mercanti, V.; Jollivet, F.; Raposo, G.; Perez, F. Synchronization of Secretory Protein Traffic in Populations of Cells. *Nat. Methods* **2012**, *9*, 493.
(52) Deka, C.; Lehnert, B. E.; Lehnert, N. M.; Jones, G. M.; Sklar, L. A.; Steinkamp, J. A. Analysis of Fluorescence Lifetime and Quenching of FITC-Conjugated Antibodies on Cells by Phase-Sensitive Flow Cytometry. *Cytometry* **1996**, *25*, 271−279.
(53) Huss, M.; Wieczorek, H. Inhibitors of V-ATPases: Old and New Players. *J. Exp. Biol.* **2009**, *212*, 341−346.
(54) Forgac, M. Vacuolar ATPases: Rotary Proton Pumps in Physiology and Pathophysiology. *Nat. Rev. Mol. Cell Biol.* **2007**, *8*, 917.
(55) Nishi, T.; Forgac, M. The Vacuolar (H+)-ATPases–Nature's Most Versatile Proton Pumps. *Nat. Rev. Mol. Cell Biol.* **2002**, *3*, 94−103.
(56) Galea, G.; Bexiga, M. G.; Panarella, A.; O'Neill, E. D.; Simpson, J. C. A High-Content Screening Microscopy Approach to Dissect the Role of Rab Proteins in Golgi-to-ER Retrograde Trafficking. *J. Cell Sci.* **2015**, *128*, 2339−2349.
(57) Klausner, R. D.; Donaldson, J. G.; Lippincott-Schwartz, J. Brefeldin A: Insights into the Control of Membrane Traffic and Organelle Structure. *J. Cell Biol.* **1992**, *116*, 1071−1080.
(58) Rzymski, T.; Petry, A.; Kračun, D.; Rieß, F.; Pike, L.; Harris, A. L.; Görlach, A. The Unfolded Protein Response Controls Induction and Activation of ADAM17/TACE by Severe Hypoxia and ER Stress. *Oncogene* **2012**, *31*, 3621−3634.
(59) Chapnick, D. A.; Bunker, E.; Liu, X. A Biosensor for the Activity of the "Sheddase" TACE (ADAM17) Reveals Novel and Cell Type−Specific Mechanisms of TACE Activation. *Sci. Signaling* **2015**, *8*, rs1.
(60) Yan, Y.; Zhang, J.; Guo, J.-L.; Huang, W.; Yang, Y.-Z. Multiple ShRNA-Mediated Knockdown of TACE Reduces the Malignancy of HeLa Cells. *Cell Biol. Int.* **2009**, *33*, 158−164.
(61) Verboogen, D. R. J.; González Mancha, N.; ter Beest, M.; van den Bogaart, G. Fluorescence Lifetime Imaging Microscopy Reveals Rerouting of SNARE Trafficking Driving Dendritic Cell Activation. *eLife* **2017**, *6*, No. e23525.
(62) Manderson, A. P.; Kay, J. G.; Hammond, L. A.; Brown, D. L.; Stow, J. L. Subcompartments of the Macrophage Recycling Endosome Direct the Differential Secretion of IL-6 and TNFα. *J. Cell Biol.* **2007**, *178*, 57−69.
(63) Eisenberg-Lerner, A.; Benyair, R.; Hizkiahou, N.; Nudel, N.; Maor, R.; Kramer, M. P.; Shmueli, M. D.; Zigdon, I.; Cherniavsky Lev, M.; Ulman, A.; Sagiv, J. Y.; Dayan, M.; Dassa, B.; Rosenwald, M.; Shachar, I.; Li, J.; Wang, Y.; Dezorella, N.; Khan, S.; Porat, Z.; Shimoni, E.; Avinoam, O.; Merbl, Y. Golgi Organization Is Regulated by Proteasomal Degradation. *Nat. Commun.* **2020**, *11*, 409.
(64) Baumann, J.; Ignashkova, T. I.; Chirasani, S. R.; Ramírez-Peinado, S.; Alborzinia, H.; Gendarme, M.; Kuhnigk, K.; Kramer, V.; Lindemann, R. K.; Reiling, J. H. Golgi Stress−Induced Transcriptional Changes Mediated by MAPK Signaling and Three ETS Transcription Factors Regulate MCL1 Splicing. *Mol. Biol. Cell* **2018**, *29*, 42−52.
(65) Oku, M.; Tanakura, S.; Uemura, A.; Sohda, M.; Misumi, Y.; Taniguchi, M.; Wakabayashi, S.; Yoshida, H. Novel Cis-Acting Element GASE Regulates Transcriptional Induction by the Golgi Stress Response. *Cell Struct. Funct.* **2011**, *36*, 1−12.
(66) Taniguchi, M.; Nadanaka, S.; Tanakura, S.; Sawaguchi, S.; Midori, S.; Kawai, Y.; Yamaguchi, S.; Shimada, Y.; Nakamura, Y.; Matsumura, Y.; Fujita, N.; Araki, N.; Yamamoto, M.; Oku, M.; Wakabayashi, S.; Kitagawa, H.; Yoshida, H. TFE3 Is a BHLH-ZIP-Type Transcription Factor That Regulates the Mammalian Golgi Stress Response. *Cell Struct. Funct.* **2015**, *40*, 13−30.
(67) Reiling, J. H.; Olive, A. J.; Sanyal, S.; Carette, J. E.; Brummelkamp, T. R.; Ploegh, H. L.; Starnbach, M. N.; Sabatini, D. M. A CREB3−ARF4 Signalling Pathway Mediates the Response to Golgi Stress and Susceptibility to Pathogens. *Nat. Cell Biol.* **2013**, *15*, 1473−1485.
(68) Sbodio, J. I.; Snyder, S. H.; Paul, B. D. Golgi Stress Response Reprograms Cysteine Metabolism to Confer Cytoprotection in Huntington's Disease. *Proc. Natl. Acad. Sci. U. S. A.* **2018**, *115*, 780−785.
(69) Taniguchi, M.; Sasaki-Osugi, K.; Oku, M.; Sawaguchi, S.; Tanakura, S.; Kawai, Y.; Wakabayashi, S.; Yoshida, H. MLX Is a Transcriptional Repressor of the Mammalian Golgi Stress Response. *Cell Struct. Funct.* **2016**, *41*, 93−104.
(70) Stransky, L.; Cotter, K.; Forgac, M. The Function of V-ATPases in Cancer. *Physiol. Rev.* **2016**, *96*, 1071−1091.
(71) Wolfe, D. M.; Lee, J.-h.; Kumar, A.; Lee, S.; Orenstein, S. J.; Nixon, R. A. Autophagy Failure in Alzheimer's Disease and the Role of Defective Lysosomal Acidification. *Eur. J. Neurosci.* **2013**, *37*, 1949−1961.
(72) Koh, J.-Y.; Kim, H. N.; Hwang, J. J.; Kim, Y.-H.; Park, S. E. Lysosomal Dysfunction in Proteinopathic Neurodegenerative Disorders: Possible Therapeutic Roles of CAMP and Zinc. *Mol. Brain* **2019**, *12*, 18.
(73) Dehay, B.; Ramirez, A.; Martinez-Vicente, M.; Perier, C.; Canron, M.-H.; Doudnikoff, E.; Vital, A.; Vila, M.; Klein, C.; Bezard, E. Loss of P-Type ATPase ATP13A2/PARK9 Function Induces General

https://doi.org/10.1021/acschembio.1c00907
ACS Chem. Biol. 2022, 17, 240−251

Lysosomal Deficiency and Leads to Parkinson Disease Neurodegeneration. *Proc. Natl. Acad. Sci. U. S. A.* **2012**, *109*, 9611−9616.
(74) Jinn, S.; Drolet, R. E.; Cramer, P. E.; Wong, A. H.-K.; Toolan, D. M.; Gretzula, C. A.; Voleti, B.; Vassileva, G.; Disa, J.; Tadin-Strapps, M.; Stone, D. J. TMEM175 Deficiency Impairs Lysosomal and Mitochondrial Function and Increases α-Synuclein Aggregation. *Proc. Natl. Acad. Sci. U. S. A.* **2017**, *114*, 2389−2394.
(75) Fernandez-Mosquera, L.; Yambire, K. F.; Couto, R.; Pereyra, L.; Pabis, K.; Ponsford, A. H.; Diogo, C. V.; Stagi, M.; Milosevic, I.; Raimundo, N. Mitochondrial Respiratory Chain Deficiency Inhibits Lysosomal Hydrolysis. *Autophagy* **2019**, *15*, 1572−1591.
(76) Bagh, M. B.; Peng, S.; Chandra, G.; Zhang, Z.; Singh, S. P.; Pattabiraman, N.; Liu, A.; Mukherjee, A. B. Misrouting of V-ATPase Subunit V0a1 Dysregulates Lysosomal Acidification in a Neurodegenerative Lysosomal Storage Disease Model. *Nat. Commun.* **2017**, *8*, 14612.
(77) Warren, S. C.; Margineanu, A.; Alibhai, D.; Kelly, D. J.; Talbot, C.; Alexandrov, Y.; Munro, I.; Katan, M.; Dunsby, C.; French, P. M. W. Rapid Global Fitting of Large Fluorescence Lifetime Imaging Microscopy Datasets. *PLoS One* **2013**, *8*, No. e70687.

https://doi.org/10.1021/acschembio.1c00907
ACS Chem. Biol. 2022, 17, 240−251